ARTICLE

Spontaneous Buckling of Lipid Bilayer and Vesicle Budding Induced by Antimicrobial Peptide Magainin 2: A Coarse-Grained Simulation Study

Hyung-June Woo* and Anders Wallqvist

Biotechnology High Performance Computing Software Applications Institute, Telemedicine and Advanced Technology Research Center, United States Army Medical Research and Materiel Command, Fort Detrick, Maryland 21702, United States

ABSTRACT: Molecular mechanisms of the action of antimicrobial peptides on bacterial membranes were studied by large scale coarse-grained simulations of magainin 2—dipalmitoylphosphatidylcholine/palmitoyloleoylphosphatidylglycerol (DPPC/POPG) mixed bilayer systems with spatial extents up to 0.1 μm containing up to 1600 peptides. Equilibrium simulations exhibit disordered toroidal pores stabilized by peptides. However, when a layer of peptides is placed near the lipid head groups on one side of the bilayer only, their incorporation leads to a spontaneous buckling of the bilayer. This buckling is followed by the formation of a quasi-spherical vesicular bud connected to the bilayer by a narrow neck. The mean curvature of the budding region is consistent with what is expected based on the dependence of the area per lipid on the peptide-to-lipid ratio in equilibrium simulations. Our simulations suggest that the incorporation of antimicrobial peptides on the exterior surface of a vesicle or a bacterial cell leads to buckling and vesicle budding, presumably accompanied by nucleations of giant transient pores of sizes that are much larger than indicated by equilibrium measurements and simulations.
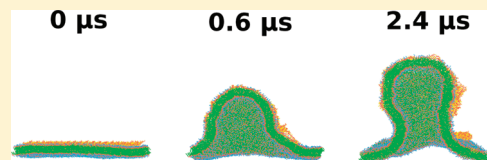
■ INTRODUCTION

Antimicrobial peptides (AMPs) are found in many organisms as part of their natural defense mechanisms against bacterial infection. The activity of AMPs arises from their interactions with lipid membranes rather than proteins, making them potential alternatives to traditional antibiotics. The AMPs are usually short and highly charged cationic α-helical peptides with amphipathic character, selectively permeabilizing bacterial lipid membranes at sufficiently high concentrations with pore formation. The exact nature of the pore formation mechanisms, however, is yet to be clarified completely. Among the models proposed,[1,2] the carpet mechanism[3,4] involves peptides adsorbed on the membrane uniformly up to a critical surface concentration, beyond which a global instability is triggered. The barrel-stave model[5−7] has transmembrane pores formed by a few AMPs lying perpendicular to the membrane—water interface with their hydrophobic faces stabilizing the pore interior. The inner surface of the pore is lined up instead by lipid head groups in the toroidal pore model,[8,9] together with the AMPs lying perpendicular to the bulk lipid surface. In the sinking raft model,[10] peptide aggregates on the surface sink into the interior maintaining their orientation perpendicular to the interface, eventually reaching the other side of the membrane. Experimental evidence so far suggests that the action of different AMPs involves varying degrees of one or multiple mechanisms among these possibilities.

Magainin 2, first isolated from the African frog *Xenopus laevis*,[11] is one of the most well-characterized AMPs. In its interactions with bacterial membranes, magainin 2 is strongly attracted toward the membrane—water interface, forming an α-helix lying parallel to the surface.[12,13] At sufficiently high concentrations, a number of these helical rods are believed to enter the membrane interior, inducing pore formation.[14] Neutron in-plane scattering experiments

of multilamellar stacks[8] and vesicles[15] suggested that these inserted peptides form toroidal rather than barrel-stave pores, and the mean diameter of these pores was estimated to be ~8 nm.[15]

The structure of equilibrated pores, however, may not completely explain the mechanism of AMP action adequately, since the exact transient route taken by systems during pore formations likely plays important roles in determining the fate of a particular membrane under attack. Indeed, recent studies have suggested that kinetic pathways to the formation of such pores may involve considerably richer structural transformations within the target membranes than suggested by equilibrated pore structures. Almeida and Pokorny found that the efflux of dyes from vesicles under magainin 2 occurs via an "all-or-none" type kinetic mechanism.[2] Giant unilamellar vesicles (GUVs) exhibit expansions of surface area under melittin concentrations[16] and rapid leakages of fluorescent dyes under magainin 2,[17,18] which appears to act on the membrane by inducing positive spontaneous curvatures.[18] When the composition of neutral-anionic lipid mixtures in the vesicles is varied, the minimum peptide concentration required for pore formation increases with decreasing membrane surface charge density.[19] In their latest study using GUVs, Tamba et al.[20] found that the time course of leakage depends on the size of fluorescent probe molecules. With small probes, a rapid initial leakage was followed by a slower regime. In contrast, larger molecules exhibited a much smaller initial phase only and were unable to leak out of vesicles completely. The estimated effective cross sectional area of the pores corresponding to the initial leakage was ~20 nm.

These results together imply the following scenario of magainin 2-induced pore formation:[20] the initial strong adsorption of magainin 2 on the external surface of the membrane causes a large imbalance of surface tension between the external and internal surfaces. The mechanical instability due to this imbalance leads to the creation of giant pores through which a large portion of peptides enter the vesicle while allowing for the massive effusion of probes. The subsequent balancing of the concentration of peptides between the external and internal surfaces reduces the pore size, which eventually reaches the level observed in equilibrium measurements in time scales up to minutes.[8]

The hypothesis that the magainin 2-induced pores initially have effective diameters much larger than relevant molecular length scales is expected to have significant implications to its overall action in vivo: the bacterial cell death caused by the pore formation could be dominated by this initial transient period, in which large transient forces disrupt the membrane. A more direct test of this hypothesis can be achieved by molecular simulation techniques, and here we report a study of magainin 2-induced membrane permeabilization based on coarse-grained (CG) molecular dynamics (MD) simulations.

Numerous MD simulations have previously been performed to investigate the interaction of AMPs with membranes. Appelt et al. have studied the concentration dependence of AMP—lipid interactions using all-atom MD.[21] Leontiadou et al. performed MD simulations of magainin-H2 in dipalmitoylphosphatidylcholine (DPPC) lipid membranes, reporting the formation of disordered toroidal pores, which involved up to four peptides that resulted in orientations perpendicular to the membrane surface.[22] This study, however, employed a mutated magainin that interacts strongly with neutral bilayers. Kandasamy and Larson have investigated the effects of salt concentrations on magainin—bilayer interactions using all-atom MD.[23] Dittmer et al. reported a combined NMR—MD study of alamethicin—lipid interactions.[24] Sengupta et al. observed significant amounts of disorder in toroidal pore structures in another MD study of AMPs.[25] Jean-Francois et al.[26] also investigated the roles of electrostatic effects on AMP action.

CG simulations greatly expand the time and length scales accessible to MD studies to ranges necessary to describe large-scale collective effects observed in experiments with high peptide concentrations. Illya and Deserno observed via solvent-free CG simulations that concerted interactions between multiple AMPs can stabilize the transmembrane orientation.[27] Other AMPs have also been investigated in a number of recent simulation studies utilizing CG techniques,[28−30] including the observation of the spontaneous formation of barrel-stave pores in LS3-DPPC systems by Gkeka and Sarkisov.[31] Rzepiela et al.[32] extended the atomistic simulation study of magainin-H2/DPPC system[22] with combined atomistic/CG simulations to find a dynamic equilibrium of peptides between surface-aligned and transmembrane states within the disordered toroidal pores.

Major advantages of CG simulations compared to atomistic studies include extensions not only in time but also in length scales. However, the formation and evolution of mesoscale spatial patterns during transient pore formations induced by AMP action have not been examined yet using CG simulation to our knowledge. In this paper, we report a CG simulation study of AMP—bilayer systems in length scales large enough to examine the transient giant pore formation suggested by recent kinetic experiments. We used the empirical CG force field MARTINI developed by Marrink and co-workers,[33−35] which is now widely used for simulating large-scale collective features of systems containing membranes. Gkeka and Sarkisov have recently evaluated the use of MARTINI force fields in characterizing the interactions between amphiphilic peptides and lipid bilayers.[36] The MARTINI force fields for lipids in particular reproduce most of the mesoscale properties of monolayers and bilayers semiquantitatively, including the gel—fluid transition of DPPC molecules (transition temperature 295 ± 5 K versus the experimental 315 K).[37] Notably, Baokina et al.[38] have elucidated the molecular mechanism of lipid monolayer collapse under lateral compression using the MARTINI force fields, revealing the important roles played by the buckling, protrusion, and budding of monolayer folds in the process.

We find the equilibrium properties of magainin 2-containing bilayers to be largely consistent with previous studies that suggested disordered toroidal pores stabilized by peptides. However, when a large number of peptides are placed only on one side of the membrane, we observe a spontaneous buckling of the bilayer via the increase of positive curvature on the magainin 2-bound surface. This buckling transition is akin to the monolayer collapse induced by lateral compression in the air—water interface.[38] Our results provide direct structure-based evidence for the important roles played by the transient giant pore formation during AMP action as suggested by recent kinetic experiments.[20]

■ METHODS

Parameters and Simulation Conditions. Magainin 2 (GIGKFLHSAKKFGKAFVGEIMNS) and mixed DPPC/palmitoyloleoylphosphatidylglycerol (POPG) bilayers were chosen to build a model of an AMP—anionic lipid membrane system, simulated using the MARTINI force field[33,35] with the corresponding parameters for DPPC and POPG.[35,38] Na^+ (or Cl^-) ions were added to neutralize each system. The GROMACS software package[39] was used for simulations. The molecules in this paper refer to the CG MARTINI versions of CG groups. The NMR structure of magainin 2 in micelles by Gesell et al. (PDB ID: 2MAG)[40] was used for the peptides. The DSSP program[41] was used to specify the secondary structure information of the peptide, which was α-helical for 18 residues. Energy minimizations were performed using the steepest descent method. MD simulations were generally performed with time steps of 0.03 ps in periodic boundary conditions with electrostatic options recommended for MARTINI[33,34] and temperature (310 K), pressure (1 bar) controls using Berendsen thermostats.[42] The pressure coupling used a relaxation time of 3.0 ps and a compressibility of 3×10^{-5} bar^{-1}.

System Setup. The mixed bilayer containing DPPC:POPG in a 4:1 ratio was built by self-assembly simulations. Single DPPC and POPG coordinates were replicated to 96 and 24 molecules, respectively, by translations, to which 3200 water and 24 Na^+ atoms were added randomly. The resulting system was energy minimized and simulated for 27 ns, which produced a well-equilibrated bilayer configuration. This mixed bilayer was replicated together with a peptide placed next to the bilayer interior. Alternate inversions of z-direction were used to minimize the bias in the placement of peptides toward the two surfaces of the bilayer to build a system with one-fourth of the compositions of system A in Table 1. Equilibration simulations were performed with constant pressure setup with the semi-isotropic scheme that allows fluctuations of lateral and perpendicular box lengths

Table 1. Configurations of Systems Simulated

	number of molecules					P/L	simulation length (μs)	dimension (nm; $x \times y \times z$)	
	magainin 2	DPPC	POPG	Na$^+$/Cl$^-$	CG water[a]			initial	final
A[b]	0	6144	1536	1536/0	204 800	0	0.6		48.0 × 48.0 × 15.1
	77	6144	1536	1305/0	204 800	0.0100	0.6		48.4 × 48.4 × 14.8
	162	6144	1536	1050/0	204 800	0.0211	0.6		49.9 × 49.9 × 14.2
	230	6144	1536	846/0	204 800	0.0299	0.6		50.3 × 50.3 × 13.0
	312	6144	1536	600/0	204 800	0.0406	0.6		51.4 × 51.4 × 13.5
	384	6144	1536	384/0	204 800	0.0500	0.6		51.5 × 51.5 × 13.5
B[c]	384	6144	1536	384/0	554 797	0.0500	2.4	48 × 48 × 36	37 × 37 × 60
C[c]	384	6144	0	0/1152	554 797	0.0625	2.1	45 × 45 × 34	34 × 34 × 66
D[c]	1600	24 576	6144	1344/0	2 301 023	0.0521	2.1	95 × 95 × 36	84 × 84 × 46
E[d]	384	5361	1387	235/0	554 797	0.0569	0.3	37 × 37 × 60	33 × 33 × 69

[a] A CG water in MARTINI force fields corresponds to four water molecules. [b] Equilibrium simulations with symmetric distributions of peptides. The box dimension refers to the final configurations (Figure 1). [c] Transient simulations started with peptides placed on one side of the bilayer only (Figure 4: B; Figure 5: C; Figure 7: D). [d] Configuration of the system containing the mini-vesicle formed by removing the neck in the final configuration of B (Figure 6).

independently. This system was simulated for 0.6 μs and replicated twice in the x- and y-directions, followed by another 1.2 μs MD to obtain the equilibrated mixed bilayer—magainin 2 configuration. The resulting system A with the peptide to lipid ratio $P/L = 0.05$ was simulated for 0.6 μs. The final configuration was used to generate a starting configuration of a system with a smaller P/L ratio by randomly deleting peptides and adjusting the number of ions, with the resulting system simulated for 0.6 μs. This procedure was repeated up to $P/L = 0$.

Fluctuations of box sizes in x- and y-directions showed adequate equilibrations after 0.2 μs. Equilibrium properties of magainin-embedded bilayers were calculated by averaging over 0.2–0.6 μs for each simulation. In calculating the distribution of magainin 2 for Figure 2A, the peptide center was defined as the center of mass of backbone atoms. The height was defined as the difference of its z-position from the bilayer center at the location in the x,y-plane. To obtain the bilayer center height, the x,y-plane was divided into grids (20 in each direction, or ~2.6 nm spacing), and the z-coordinates of phosphate groups within each grid were averaged. The angle of peptide orientation in Figure 2B was defined as that of the vector connecting the two backbone atoms of Gly1 and Ser23 with respect to the z-axis (modulo 90°). The phosphate group distributions in Figure 3A were calculated by similar averages of phosphate heights with respect to the bilayer center over the x, y-plane grids. The two curves for $P/L = 0.05$ and 0 were shifted such that their central minima would be located at $z = 0$.

For the transient membrane buckling simulations, the pure bilayer ($P/L = 0$) configuration was used to prepare extended bilayers. For system B, a slab of water molecules was placed on top of the pure bilayer and equilibrated for 0.6 μs prior to the placement of peptides. To build system D, the extended bilayer used for B was replicated twice in the x- and y-directions and equilibrated. A single magainin 2 configuration was replicated into x- and y-directions with spacings chosen such that the peptides would cover the membrane—water interface. Each peptide was then translated vertically so that its center would be positioned 1 nm above the closest phosphate group of the bilayer, producing an undulating peptide layer that uniformly covered the hydrophilic region near the solvent interface. Water molecules closer than 0.5 nm to peptide atoms were then deleted. The systems were energy minimized, equilibrated for 0.6 μs, and

simulated for periods indicated in Table 1. In Figures 4, 5, and 7, a small fraction of atoms have been translated based on the periodic boundary condition such that the bilayer appears as a single piece. None of the nonsolvent atoms were closer to the periodic images of others along the z-direction than 10 nm. The pure DPPC bilayer—peptide system (system C in Table 1) was prepared by first deleting POPG lipids from the initial configuration of the system B bilayer without peptides. The pure DPPC bilayer was then equilibrated and peptides were placed similarly.

For the simulation of vesicle formation from the disconnected bud, the lipid molecules in the neck region (between 10 and 20% of the box length in the z-direction from the bottom) were deleted, and the number of ions was adjusted. The lipids inside the vesicle were classified into the inside and outside groups by calculating the distance of phosphates from the center of mass. The radii of the outside and inside groups were obtained by averaging the maximum distance from each phosphate to others in the same group.

RESULTS AND DISCUSSION

Magainin 2 Forms Disordered Toroidal Pores in Equilibrium. Equilibrium model bilayers containing DPPC:POPG in 4:1 ratio and magainin 2 peptides were built and simulated in order to examine the stable pore morphologies and large-scale collective effects of these peptides on bilayer properties. The parameters, lipid composition, and temperature (310 K) are those that have been used successfully to describe lipid monolayer collapse by Baoukina et al.[38] In building these systems, peptides were placed in the interior of the membrane parallel to the lipid tail groups before equilibration, such that they would sample relatively rare transmembrane configurations more efficiently, and result in peptide distributions that are roughly equal on both sides of the membrane. Figure 1 shows an example of the equilibrated configurations with $P/L = 0.05$, which corresponds to a surface concentration threshold above which pore formations on GUVs become accelerated.[19] Most of the peptides on the surfaces ended up in clusters containing transmembrane pores, which appeared to perturb the bilayers significantly (Figure 1A,B). The representative pore structure shown in Figure 1C clearly indicates the disordered toroidal morphology, where peptides lining up the pore wall are surrounded by a
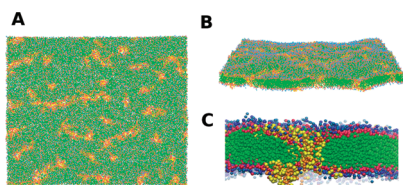
Figure 1. Equilibrated bilayer configuration (DPPC:POPG = 4:1) containing magainin 2 at the peptide-to-lipid ratio of $P/L = 0.05$. See Table 1 (system A) for number of molecules and dimensions. In C, a representative pore stabilized by the peptides is shown in greater detail. Color schemes are as follows: PO_4 and NC_3 atoms of lipids in blue, GL groups of POPG in red, lipid tail carbon atoms in green, peptide side chains in yellow, and peptide backbone groups in orange. For clarity, CG water groups are not shown.
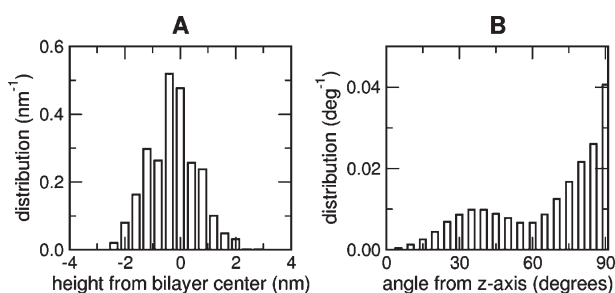
Figure 2. Equilibrium properties of the pores formed in magainin 2-imbedded bilayers. A and B show the distributions of peptide center and orientation within the bilayer, respectively, at $P/L = 0.05$ (see Figure 1).

Figure 3. Modification of bilayer properties by magainin 2. (A) Distribution of phosphate groups within the membrane for peptide-free and $P/L = 0.05$ cases. The probability distribution is normalized such that the total area under the curve equals 1. (B) Dependence of area per lipid on P/L. The dashed line is a linear fit $(area/nm^2 = 0.598 + 2.081\ P/L)$.

substantial amount of lipid head groups drawn into the bilayer interior. The distribution of peptide centers of mass (Figure 2A) suggests that at peptide concentrations relevant to membrane disruption, magainin 2 are distributed widely over the pore interior including its center. On the other hand, their orientation with respect to the bilayer surface (Figure 2B) exhibits a bimodal distribution with two possible orientations, one parallel to the surface ($\sim 90°$), and another near $\sim 30°$. The distribution near the orientation parallel to the surface is sharp but smaller in fraction, consistent with the expectation that they would appear within the tail parts of the positional distribution of Figure 2A.

The incorporation of peptides into the bilayer in the form of these toroidal pores leads to modifications of its overall equilibrium properties. The distribution of lipid head parts (phosphate groups) across the bilayer (Figure 3A) indicates that as magainin 2 molecules bind and form pores, the bilayer becomes thinner while increasing the density of head groups at the bilayer center, consistent with the toroidal nature of pore morphology suggested in Figure 1C. The thinning of bilayer thickness upon AMP addition has widely been observed experimentally,[16,43] including magainin 2-containing bilayers.[44] The main cause of such thinning effects is the expansion of the total surface area of bilayers containing AMPs, which we also directly observe in Figure 3B, where the area per lipid is seen to increase linearly with increasing P/L.

Our large-scale equilibrium simulation results for $P/L = 0.05$ are consistent with previous experimental and simulation studies that provided evidence for the formation of disordered toroidal pores at high concentrations of magainin 2 in bilayers with net negative surface charge densities. Ludtke et al. performed neutron in-plane scattering experiments[8] to show that the pores formed by magainins are much larger in size than can be

explained by the barrel-stave, proposing the toroidal pore model. In atomistic MD simulations by Leontiadou et al[22] of magainin H2–DPPC systems containing up to four peptides, spontaneous formations of such disordered toroidal pores were observed within 0.25 μs. The equilibrium pore structure we observe (Figure 1C) is largely consistent with the previously noted atomistic as well as the combined atomistic-CG results.[32] The latter study, in particular, showed a similar increase in phosphate group density at the bilayer center as well as the thinning of bilayer thickness on magainin-H2 addition to the neutral DPPC bilayer. Our results greatly extends the length scale of the system under consideration (from ~ 4 peptides to ~ 400) and show that the equilibrium properties observed in CG simulations using MARTINI force fields remain applicable with more experimentally relevant magainin 2–anionic lipid bilayer systems. Nevertheless, the kinetics of pore formation we deduce from our study (see below) is quite distinct from what was suggested in the simulation of the modified magainin-H2 and neutral bilayer.

Asymmetric Magainin 2 Incorporation Leads to Buckling. When a bacterial cell is exposed to high concentrations of AMPs, the peptides will initially have to bind to the outer layers of the membrane only. This asymmetry is expected to cause significant differences in the kinetic behavior of bilayer morphology changes compared to what is observed in equilibrium conditions. In order to simulate these kinetic changes and infer their implications to the mechanism of AMP action, we prepared a system of mixed bilayer with a large vertical extension and placed a layer of magainin 2 molecules on top of one side of the lipid–water interface (Figure 4). The peptides quickly became incorporated into the headgroup regions with a moderate degree of aggregation. However, the bilayer soon developed a positive curvature, with the curved regions of the bilayer eventually coalescing into a vesicular bud in ~ 0.6 μs. The budding protrusion was coated with peptides on the outer surface and remained connected to the bilayer with a neck. The growth of the protrusion was essentially complete within ~ 1 μs, and the system remained stable for another ~ 1 μs. During this buckling/budding process, the dimension of the system changed with a large decrease and increase in sizes in the x-, y-, and z-directions, respectively (Table 1).

The peptides remained strongly associated with membrane head groups in all of our simulations. This strong attractive interaction allows our simulation setup to maintain the asymmetry of peptide concentrations across the bilayer even under severe distortions. Alternative setups such as placing two bilayers within the unit cell under periodic boundary conditions often used for simulating ion transport are therefore not necessary for
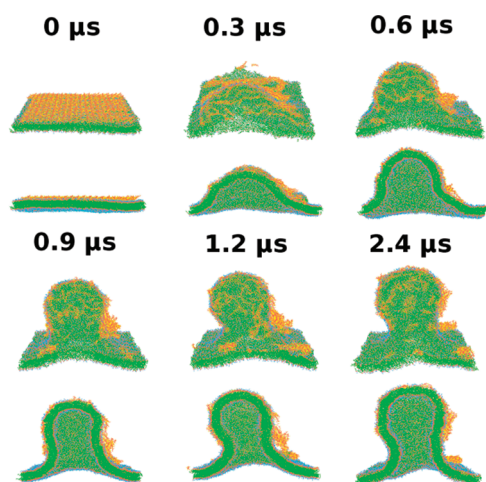
Figure 4. Vesicular budding from the bilayer (DPPC:POPG=4:1) with magainin 2 (yellow) adsorbed on one side (System B in Table 1). For each time snapshot, the bottom figure shows the cross-sectional view.

Figure 5. Vesicular budding from the pure DPPC bilayer with magainin 2 placed on one side (system C in Table 1).

our system. However, we did find that large scale changes in the aspect ratio accompanying the buckling process may produce configurations in which periodic images of one monolayer approach the other, which can allow peptide redistributions across the bilayer. We therefore chose the initial configurations for the transient simulations to be sufficiently large in order to avoid such artifacts.

The spontaneous buckling observed with asymmetric binding of peptides has previously been postulated based on many kinetic experiments of AMP action on negatively charged bilayers.[16,17,19,20] Tamba and Yamazaki observed that GUVs with nonspherical (such as prolate) shapes develop narrowing necks and evolve into dumbbell and necklace-shaped objects when exposed to increasing concentrations of magainin 2 on their exterior surfaces.[17] Such shape changes can be explained by the increase in effective surface area of the outer membrane due to the binding of peptides. In equilibrium experiments[44] and simulations (Figure 3), the expansion occurs symmetrically on both sides of the bilayer, which preserves its planar average geometry. In contrast, when the area increase is induced only on one interface of the bilayer as in a nonspherical GUV placed inside a magainin 2 solution, the difference in area across the bilayer must be accommodated by shape changes under the constraint of constant enclosed volume. These morphological changes can be described effectively by the continuum elastic descriptions of vesicles such as the area-difference elasticity model,[45] which predicts budding transitions via the growth of protrusions, narrowing of necks, and the eventual fission of the daughter cells as has indeed been observed in GUV experiments.[17] Lee et al. also have directly noted morphology changes of GUVs in melittin solution, where protrusions developed into micropipets holding the vesicles.[16]

Our transient buckling simulations confirm the driving force of such morphology changes (unbalanced expansion due to asymmetric peptide adsorption) by connecting molecular level features to the mesoscale phenomenon. The periodic boundary condition imposed in the simulation replaces the constant volume constraint of GUVs in experiments. The growth of the protrusion into a vesicular bud connected to the base bilayer that roughly remains planar can be interpreted as a result of the optimization of the free energy under this boundary condition constraint.
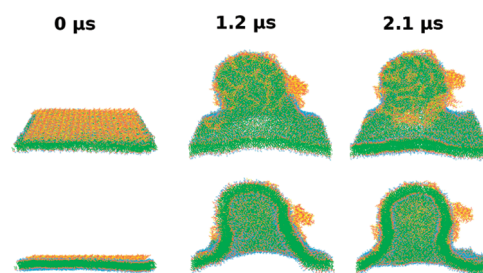
To examine the extent to which this buckling process depends on lipid compositions, we have performed a similar simulation with a bilayer consisting of DPPC only (Figure 5). The morphological shape change and its time scale are similar to those observed for the charged bilayer in Figure 4. This result suggests that the global net charge of the bilayer does not play important roles for the buckling process simulated, where a planar layer of peptides are placed near the headgroup of a monolayer, mimicking high initial surface concentrations of peptides. In GUV experiments, decreasing the surface charge density of the bilayer (or increasing the salt concentration) leads to increases both in the magainin 2 concentration in the buffer required for the pore formation as well as its time scale.[19] The fact that the artificial placement of peptides near the monolayer headgroup leads to buckling irrespective of lipid composition implies that the selectivity of magainin-induced pore-formation for charged membranes is largely based on the net long-range attraction between individual peptides and the bilayer rather than their collective action near contact. For neutral or weakly charged bilayers, the gradual adsorption and accumulation of peptides on the outer monolayer as modeled by the initial configurations of Figures 4 and 5 would either be impossible or require higher peptide concentrations and time scale.

Experiments have also indicated that the key parameter that determines the rate of pore formation is the mole fraction X_b of peptides within the bilayer rather than the ratio of bulk magainin concentration to lipid concentration, with the critical $X_b \sim 0.05$.[19] However, since in our simulations practically all peptides remain tightly incorporated into the bilayer, the P/L value we used should be interpreted as a measure of surface rather than bulk concentration ($X_b = 0.0476$ for Figures 4 and 7). Our simulated system therefore roughly corresponds to the threshold regime in GUV experiments where the effective peptide concentration in the bilayer begins to cause a large increase in the leakage rate.

A Spherical Mini-Vesicle Forms When the Neck Is Removed. The stabilization of the neck thickness to a relatively large value reflects the fact that the fission of vesicles across the point of singularity in continuum descriptions[45] involves a high free energy barrier associated with a simultaneous reversal of orientations of a large number of lipid molecules inside the bilayer. This activation process usually is catalyzed by proteins in cellular in vivo conditions.[46] These proteins (clathrins) assemble themselves into coats on the surface of the bilayer, inducing budding and fission. Kozlovsky and Kozlov studied the energetics of this fission process using elastic models and estimated the barrier to be on the order of $\sim 100\, k_B T$.[47] The CG simulation
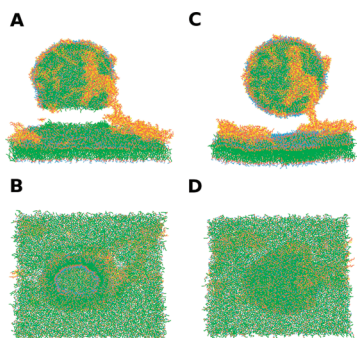
Figure 6. Spontaneous stabilization of a mini-vesicle from a disconnected bud. The initial configuration (A, B each showing the side and bottom views) was generated by deleting lipid molecules in the neck region from the configuration at 2.4 μs of Figure 4 (shown here rotated clockwise by 90°). C and D show the configuration after 0.3 μs. See Table 1 for the system compositions and dimensions (System E).

Figure 7. Vesicular budding from a peptide-containing bilayer system twice as large as that in Figure 4. See Table 1 for system composition and dimensions (system D).

result shown in Figures 4 and 5 suggests that AMPs including magainin 2 may act in ways similar to these fission proteins by bending the bilayer into small buds. The actual fission of these buds, however, would have to be activated by rare but nonnegligible thermal fluctuations.

To examine whether such mini-vesicles with diameters of tens of nanometers can indeed form as a result of AMP action when the fission free energy barrier is overcome, we removed lipid molecules in the neck region of the vesicular bud (Figure 6). Both the disconnected bud and the base membrane rapidly healed their openings, producing a spherical mini-vesicle coated with peptides and a bilayer containing the remaining fraction of magainin 2. The resulting vesicle contained 239 peptides, and 1280 and 1808 lipids in the internal and external surfaces, respectively. The radii of the internal and external monolayers were r_{in} = 7.56 nm and r_{out} = 11.40 nm, respectively. The area per lipid is therefore $4\pi \left(r_{in}{}^2 + r_{out}{}^2 \right)/(1280 + 1808) = 0.761$ nm², and P/L = 0.077. The equilibrium relationship shown in Figure 3B, on the other hand, predicts 0.758 nm² for the same P/L, in good agreement with the actual geometry. For comparison, the initial configuration of the flat bilayer in Figure 4 had an area per lipid of ~0.59 nm². The fact that the spherical vesicle derived from our CG simulations started from a flat bilayer has geometries expected from equilibrium properties further supports the conclusion that the spontaneous buckling and subsequent morphological evolution are driven by the energetic penalty associated with the surface tension imbalance across the bilayer.

The Size of Vesicular Bud Is Independent of System Sizes. In order to test how the simulated system size affects this protrusion process, we examined the time evolution of a system that is twice the size in the x- and y-directions at the same P/L value (Figure 7). A buckling process similar to that in Figure 4 was observed over the course of ~1 μs, which again produced a vesicular bud after ~2 μs with a radius of ~10 nm. The fact that doubling the size of the overall simulation cell with the same P/L value leaves the size of the vesicular bud unchanged suggests that the periodic boundary condition imposed on simulations does not substantially alter the physical mechanism behind the budding process.

This larger system had the spatial extension approaching 0.1 μm for the size of bilayer and contained 1600 magainin 2 peptides, making it roughly 2 orders of magnitude larger than any previous simulation studies of AMP−bilayer systems. This
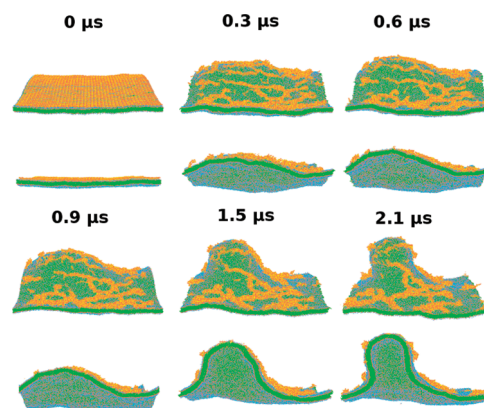
spatial extent nevertheless still covers less than ~10% of a single GUV or a bacterial cell that is on the order of ~1 μm in size. However, for spherical GUVs for which global morphological changes into shapes such as dumbbells or necklaces are not directly accessible, it is expected that the poration process will occur locally on the surface while the overall spherical morphology of the vesicle is still maintained: experimental studies of GUVs of ~10 μm diameter[20] revealed no discernible changes to the vesicle shape even after a profuse leaking has already been initiated. Our simulation results suggest a possible mechanism in which such transient pores may initially form on the surface: the growing imbalance in surface tensions between the exterior and interior surfaces from peptide binding begins to instigate buckling of bilayers. The volume of the vesicle and the average surface area of the enclosing sphere, however, are constrained, which do not allow the contraction of the sort evident in simulations shown in Figures 4, 5, and 7 where box sizes in the x- and y-directions shrink as the vesicular protrusion develops. The buckling and protrusion, nevertheless, can occur if pores of similar sizes are formed in neighboring regions within the bilayer. Such pore formations in bilayers require crossing the nucleation barrier beyond which the line tension is overcome by the membrane tension.[48] The AMPs on the surface can lower the tension and reduce the critical radius. A rare thermal activation would still be necessary to cross the barrier, which is consistent with the experimental observation that the initiation of leakage on single GUVs under high concentrations of magainin 2 is highly stochastic, with waiting times on the order of ~100 s.[20]

We have also simulated the same system under constant area (box sizes in the x- and y-directions fixed) conditions to see to what extent such a nucleation of pores might be accessible via unconstrained simulations. A moderately perturbed bilayer shape (similar to the 0.3 μs configuration in Figure 7) persisted up to ~1.2 μs with little changes in its degree of buckling, consistent with a high free energy barrier of pore nucleation. We note, however, that many other factors beyond the reach of CG simulations may contribute significantly to the pore formation mechanism: for instance, during the long waiting time periods (~100 s) prior to the activated pore formation event, appreciable amounts of water may diffuse across the membrane, allowing for changes in GUV volume and surface area. Simulation studies using different schemes of boundary conditions designed to probe such effects may offer further insight into the precise mechanism of pore formation.

Nevertheless, it is particularly notable that the experimentally estimated mean radius of the giant transient pores that form initially ($\sim$20 nm)[20] is similar to the length scale of vesicular protrusions we observe in Figures 4 and 7. In the GUV experiments, the bulk of leakage occurs after the initial giant pore formation, followed by the gradual decrease of the pore radius to levels observed in equilibrium measurements. The two very different classes of bilayer disruption we show in Figure 1 and in Figures 4, 5, and 7, one in equilibrium where the peptides are symmetrically distributed within the toroidal pores, and the other where they cause violent buckling/budding (accompanied by giant pore formations), provide strong supporting evidence for the hypotheses put forward in recent kinetic experiments.[16,19,20]

■ CONCLUSIONS

Although equilibrium structures of pores formed by AMPs in bilayers have been studied widely both in experiments and simulations, the nature of kinetic routes a vesicle or a bacterial cell experience when under attack by such peptides has received relatively less attention. Recent experiments using single GUVs have suggested that the initial pore formation responsible for the bulk of leakage involves length scales much larger than those indicated by the equilibrium structures. In our study, we greatly extended the length scale of simulations from levels of previous works on AMPs such that the relevant mesoscale collective effects can be observed directly. The results obtained provide direct structural and kinetic evidence supporting the roles played by such nonequilibrium effects in AMP action: the imbalance of surface concentrations across the bilayer provides the driving force for large scale structural instabilities, which may lead to buckling, budding, and nucleation of giant pores.

■ AUTHOR INFORMATION

Corresponding Author
*Tel: 301-619-1976. FAX: 301-619-1983. E-mail: woo@bioanalysis.org.

■ ACKNOWLEDGMENT

■ REFERENCES

(1) Bechinger, B. *Curr. Opin. Colloid Interface Sci.* **2009**, *14*, 349.
(2) Almeida, P. F.; Pokorny, A. *Biochemistry* **2009**, *48*, 8083.
(3) Shai, Y. *Biopolymers* **2002**, *66*, 236.
(4) Papo, N.; Shai, Y. *Peptides* **2003**, *24*, 1693.
(5) Huang, H. W.; Wu, Y. *Biophys. J.* **1991**, *60*, 1079.
(6) Sansom, M. S. P. *Eur. Biophys. J.* **1993**, *22*, 105.
(7) He, K.; Ludtke, S. J.; Worcester, D. L.; Huang, H. W. *Biophys. J.* **1996**, *70*, 2659.
(8) Ludtke, S. J.; He, K.; Heller, W. T.; Harroun, T. A.; Yang, L.; Huang, H. W. *Biochemistry* **1996**, *35*, 13723.
(9) Matsuzaki, K.; Murase, O.; Fujii, N.; Miyajima, K. *Biochemistry* **1996**, *35*, 11361.
(10) Pokorny, A.; Almeida, P. F. *Biochemistry* **2004**, *43*, 8846.
(11) Zasloff, M. *Proc. Natl. Acad. Sci. U.S.A.* **1987**, *84*, 5449.
(12) Matsuzaki, K.; Murase, O.; Tokuda, H.; Funakoshi, S.; Fujii, N.; Miyajima, K. *Biochemistry* **1994**, *33*, 3342.
(13) Ludtke, S. J.; He, K.; Huang, H. W. *Biochim. Biophys. Acta* **1994**, *1190*, 181.
(14) Nguyen, K. T.; Le Clair, S. V.; Ye, S.; Chen, Z. *J. Phys. Chem. B* **2009**, *113*, 12358.
(15) Han, M.; Mei, Y.; Khant, H.; Ludtke, S. J. *Biophys. J.* **2009**, *97*, 164.
(16) Lee, M.-T.; Hung, W.-C.; Chen, F.-Y.; Huang, H. W. *Proc. Natl. Acad. Sci. U.S.A.* **2008**, *105*, 5087.
(17) Tamba, Y.; Yamazaki, M. *Biochemistry* **2005**, *44*, 15823.
(18) Matsuzaki, K.; Sugishita, K.-i.; Ishibe, N.; Ueha, M.; Nakata, S.; Miyajima, K.; Epand, R. M. *Biochemistry* **1998**, *37*, 11856.
(19) Tamba, Y.; Yamazaki, M. *J. Phys. Chem. B* **2009**, *113*, 4846.
(20) Tamba, Y.; Ariyama, H.; Levadny, V.; Yamazaki, M. *J. Phys. Chem. B* **2010**, *114*, 12018.
(21) Appelt, C.; Eisenmenger, F.; Kuhne, R.; Schmieder, P.; Soderhall, J. A. *Biophys. J.* **2005**, *89*, 2296.
(22) Leontiadou, H.; Mark, A. E.; Marrink, S. J. *J. Am. Chem. Soc.* **2006**, *128*, 12156.
(23) Kandasamy, S. K.; Larson, R. G. *Biochim. Biophys. Acta* **2006**, *1758*, 1274.
(24) Dittmer, J.; Thogersen, L.; Underhaug, J.; Bertelsen, K.; Vosegaard, T.; Pedersen, J. M.; Schiott, B.; Tajkhorshid, E.; Skrydstrup, T.; Nielsen, N. C. *J. Phys. Chem. B* **2009**, *113*, 6928.
(25) Sengupta, D.; Leontiadou, H.; Mark, A. E.; Marrink, S. J. *Biochim. Biophys. Acta* **2008**, *1778*, 2308.
(26) Jean-Francois, F.; Elezgaray, J.; Berson, P.; Vacher, P.; Dufourc, E. J. *Biophys. J.* **2008**, *95*, 5748.
(27) Illya, G.; Deserno, M. *Biophys. J.* **2008**, *95*, 4163.
(28) Bond, P. J.; Parton, D. L.; Clark, J. F.; Sansom, M. S. *Biophys. J.* **2008**, *95*, 3802.
(29) Thogersen, L.; Schiott, B.; Vosegaard, T.; Nielsen, N. C.; Tajkhorshid, E. *Biophys. J.* **2008**, *95*, 4337.
(30) Lee, H.; Larson, R. G. *J. Phys. Chem. B* **2008**, *112*, 7778.
(31) Gkeka, P.; Sarkisov, L. *J. Phys. Chem. B* **2009**, *113*, 6.
(32) Rzepiela, A. J.; Sengupta, D.; Goga, N.; Marrink, S. J. *Faraday Discuss.* **2010**, *144*, 431.
(33) Marrink, S. J.; Risselada, H. J.; Yefimov, S.; Tieleman, D. P.; de Vries, A. H. *J. Phys. Chem. B* **2007**, *111*, 7812.
(34) Monticelli, L.; Kandasamy, S. K.; Periole, X.; Larson, R. G.; Tieleman, D. P.; Marrink, S. J. *J. Chem. Theory Comput.* **2008**, *4*, 819.
(35) Marrink, S. J.; de Vries, A. H.; Mark, A. E. *J. Phys. Chem. B* **2004**, *108*, 750.
(36) Gkeka, P.; Sarkisov, L. *J. Phys. Chem. B* **2010**, *114*, 826.
(37) Marrink, S. J.; Risselada, J.; Mark, A. E. *Chem. Phys. Lipids* **2005**, *135*, 223.
(38) Baoukina, S.; Monticelli, L.; Risselada, H. J.; Marrink, S. J.; Tieleman, D. P. *Proc. Natl. Acad. Sci. U.S.A.* **2008**, *105*, 10803.
(39) Lindahl, E.; Hess, B.; van der Spoel, D. *J. Mol. Model.* **2001**, *7*, 306.
(40) Gesell, J.; Zasloff, M.; Opella, S. J. *J. Biomol. NMR* **1997**, *9*, 127.
(41) Kabsch, W.; Sander, C. *Biopolymers* **1983**, *22*, 2577.
(42) Berendsen, H. J. C.; Postma, J. P. M.; van Gunsteren, W. F.; Dinola, A.; Haak, J. R. *J. Chem. Phys.* **1984**, *81*, 3684.
(43) Lee, M.-T.; Chen, F.-Y.; Huang, H. W. *Biochemistry* **2004**, *43*, 3590.

(44) Ludtke, S.; He, K.; Huang, H. *Biochemistry* **1995**, *34*, 16764.

(45) Miao, L.; Seifert, U.; Wortis, M.; Dobereiner, H.-G. *Phys. Rev. E* **1994**, *49*, 5389.

(46) Kirchhuausen, T. *Nat. Rev. Mol. Cell Biol.* **2000**, *1*, 187.

(47) Kozlovsky, Y.; Kozlov, M. M. *Biophys. J.* **2003**, *85*, 85.

(48) Karatekin, E.; Sandre, O.; Guitouni, H.; Borghi, N.; Puech, P. H.; Brochard-Wyart, F. *Biophys. J.* **2003**, *84*, 1734.